OPEN ACCESS

University of Dundee

University of Dundee

Microanalysis of hybrid characterization of PLA/cHA polymer scaffolds for bone regeneration

Oladapo, Bankole I.; Daniyan, Ilesanmi A.; Ikumapayi, Omolayo M.; Malachi, Olaoluwa B.; Malachi, Idowu O.

Link to publication in Discovery Research Portal

Citation for published version (APA):
Oladapo, B. I., Daniyan, I. A., Ikumapayi, O. M., Malachi, O. B., & Malachi, I. O. (2020). Microanalysis of hybrid characterization of PLA/cHA polymer scaffolds for bone regeneration. *Polymer Testing*, *83*, [106341]. https://doi.org/10.1016/j.polymertesting.2020.106341
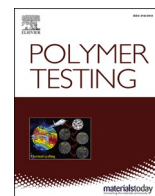
Material Properties

Microanalysis of hybrid characterization of PLA/cHA polymer scaffolds for bone regeneration

Bankole I. Oladapo [a,*], Ilesanmi A. Daniyan [b], Omolayo M. Ikumapayi [c], Olaoluwa B. Malachi [d], Idowu O. Malachi [e]

[a] School of Engineering and Sustainable Development, De Montfort University Leicester, UK
[b] Department of Industrial Engineering, Tshwane University of Technology, Pretoria, South Africa
[c] Department of Mechanical Engineering Science, University of Johannesburg, Johannesburg, South Africa
[d] Computer Science and Engineering, Obafemi Awolowo University, Ile-Ife, Nigeria
[e] Department of Mechanical EngineeringEkiti StateUniversityAdo-EkitNigeria, Nigeria

A B S T R A C T

Tissue engineering uses some engineering strategies for the reconstruction and repair of the compromised tissues, among which the use of biomaterials as an alternative to conventional transplants is significant. However, not many research has been developed on the use of biopolymer nanostructure microanalysis and calcium phosphate composites of carbon apatite in PLA as scaffolds for tissue regeneration. In this work, poly (lactic acid) filaments with 5% and 20%, carbon apatite (cHA) were microanalysis to produce a 3D printing scaffold. The scaffolds were characterised by the Scanning Electron Microscope (SEM) and Energy Dispersive X-Ray (EDX) techniques, thereby making it possible to notice a good load dispersion. The microstructural analysis of the scaffolds was carried out by computerised micro-tomography to determine the roughness, morphological parameters of pore size distribution, porosity, as well as better visualisation of the distribution of particles. A computational in vitro and microanalysis tests to assess the biocompatibility viability of the PLA/cHA structure with a variation of scaffold geometry to evaluate their effects on morphological, physicochemical and mechanical properties were also carried out. The characterisation of Ca and P release assays were observed for longer incubation times and the dynamic condition control to simulate the stresses suffered by the biomaterial exerted by the flow of fluids was achieved. The results obtained indicated that the micrographs of the cross-sections of the scaffolds showed a flatness in the loaded material when compared to the 100/0 PLA. Furthermore, the apparent porosity of 5% and 20% of cHA scaffolds gave a porosity percentage of approximately 62% and 41% respectively. The reduced summit height, reduced valley depth and the percentage upper and lower bearing area difference of the samples are 16.33 nm, 9.62 nm and 75.07% respectively. The morphological characterisation surface roughness analysis and tolerance insertion gave a favourable reduced porosity result for the composite scaffolds with 5% of cHA. Hence, this work will assist biomaterial industries in the development of biomaterials which have been engineered with biological systems to meet medical purposes.

1. Introduction

Advances in medicine in recent decades have enabled growth in the life expectancy of the world population. Over the years, the performance of human organs, tissues and the whole organism are naturally compromised. This compromise makes it necessary to use medical interventions in the reconstruction and repair of tissues damaged by injuries resulting from factors such as the reduction in mechanical resistance. Thus, maintaining the health of individuals become

indispensable, resulting in a stimulus for several studies in Additive Manufacturing [1,2]. Tissue engineering uses some engineering strategies for the reconstruction and repair of these compromised tissues; among these is the use of biomaterials as scaffolds that support the regeneration of damaged tissue [1,2]. Biocompatible polymers are materials aimed at the development of frameworks for bone regeneration, among which, the polylactic acid (PLA) is highlighted by its safety history when used in the human clinic [2]. However, such materials are known to have low mechanical strength when compared to other classes

---

of biomaterials [3,4]. To overcome this deficiency and to improve biocompatibility, there is the need to add properties such as bioactivity and osteointegration to these materials. Studies have been developed using inorganic fillers in biopolymer matrices for the production of frameworks. Furthermore, calcium phosphates, such as hydroxyapatite (HA), are usually used to perform such roles because they are biocompatible, bioactive and have a composition similar to the inorganic fraction of bone, thus, favouring and assisting the regeneration of damaged tissue [4]. Due to its low reabsorption rate, studies are carried out to modify hydroxyapatite to improve its reabsorption. These studies include the replacement of the phosphate groups (PO_4^{-3}) by the carbonate groups (CO_3^{-2}), which changes the crystalline structure of HA, thereby, increasing its solubility and favouring resorption by osteoblasts. The poxy-substituted hydroxyapatite edited by CO_3^{-2} is referred to as the carbonated hydroxyapatite (cHA) [5,6].

Polylactic acid (PLA) is a polyester commercially obtained by condensing the hydroxyl and carboxyl groups of the lactic acid monomer or by opening the lactide ring [7–9]. It has two forms that are optical isomers: L-lactic acid and lactic acid, as shown in Fig. 1. PLA is obtained by the monomer in the L-lactic acid form, while the PDLA is achieved by the monomer in the D-lactic acid form. The PDLLA is achieved by the combination of the optical isomers L-lactic acid and D-lactic acid. The PLLA has higher molar mass, degree of crystallinity, stiffness and better mechanical properties than the PLDA [10,11]. The PLA is a biocompatible and biodegradable polymer whose biodegradation occurs by hydrolysis in the chain breaking stages with oligomer formation, lactic acid formation and lactic acid absorption by enzymes in the Kreb's cycle region of aerobic cellular metabolism. In the environment, the lactic acid formed is decomposed into CO_2 and H_2O in periods less than two years [12,13]. In the case of using PLA as a biomaterial, its degradation depends on some characteristics such as the degree of crystallinity, molar mass, type of isomerism and also the implant site due to pH change [14–16]. In addition to its biocompatibility and biodegradability, PLA is a polymer with low rigidity, excellent processability and thermal stability [17,18]. Calcium phosphates are essential components of bone tissue that participate in bone regeneration through the

mineralisation cycle. They have properties of bioactivity, osteointegration and composition similar to the bone mineral part [19,20]. Hydroxyapatite ([Ca_{10} (PO_4)$^6OH_2$]) is hydrated crystalline calcium phosphate, with high stability in an aqueous medium. It has a Ca/P molar ratio of 1.67. The crystalline structure of its unit cell is compact hexagonal, with lattice parameters measuring 9.42 Å and c measuring 6.88 Å, having ten Ca^{2+} ions located at the non-parallel sites. The Ca^1 site allocates four Ca^{2+}ions in a column, and the Ca^2 site assigns six Ca^{2+} ions aligned in an equilateral triangle which is perpendicular to the c axis of the plane, where the OH groups lie [21–24]. The production of 3D material biopolymer matrix scaffolds from the hybrid materials has been the focus of promising studies in tissue engineering. Thermoplastic biopolymer matrix frameworks are successfully developed by the 3D melt deposition modelling (FDM) printing technique. The success of fabrication of such structures is attributed to the fact that the technology is a fast, cost-effective and better-performing alternative in the production of customised and highly complex parts when compared to the conventional manufacturing methods such as particulate evaporation of solvent [25–27]. Many works have been reported on the development of bio-nanocomposites for biomedical engineering applications. For instance, Ilyas et al. [28] experimented with sugar palm nano fibrilated cellulose investigating the effect of the different cycles on the yield and the physicochemical, morphological as well as the thermal behaviour of the biomaterial. The result obtained indicated that the nanofabricated cellulose has the potential for use in tissue engineering scaffolds, bio-parking and filtration media. Also, Sanyang et al. [29] developed sugar palm starch-based composites for packing applications. The findings of the work indicate that the use of the biomaterial is eco-friendly and can substitute for the use of plastics in packing applications, thereby, solving the disposal problems of plastics. Furthermore, Arockianathan et al. [30] evaluated the biocomposite films which contains alginate and sago stain impregnated with silver nanoparticles while Atikah et al. [31] investigated the degradation and physical properties of sugar palm starch and sugar palm fibrillated cellulose biocomposites. The results obtained from these work demonstrated the suitability of the biomaterial for the development of tissue engineering
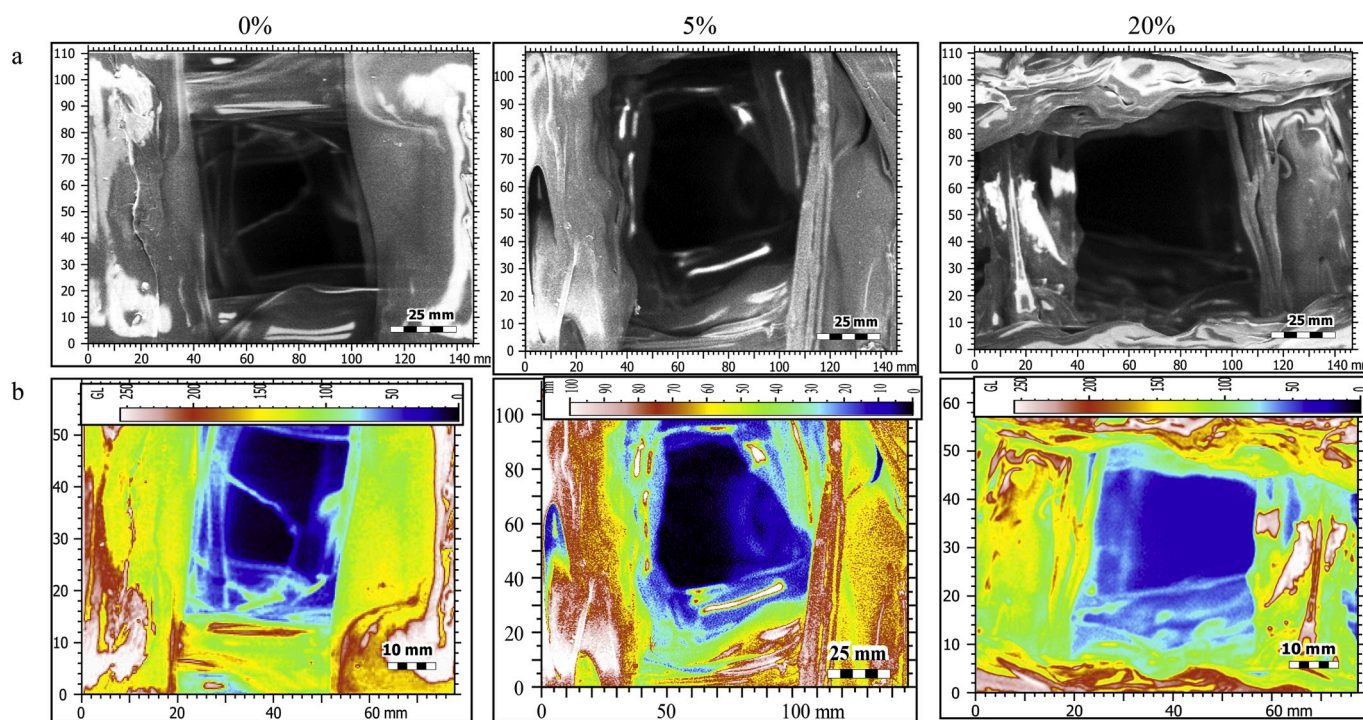

Fig. 1. (a) Illustrates the tetragonal symmetry of the deposited scaffolds with its simple width length and height periodic structure (b) is a 3D radial structure of the deposited scaffold having a joint centre.

scaffolds. In addition, Glowinska and Datta [32] developed a novel bio-based polyurethane composites with microcrystalline cellulose. The analysis of the results obtained from the structural, morphological and mechanical behaviour of the biomaterial indicates that it is suitable for biomedical application. Although, many works have been reported on the use of biomaterials as an alternative to conventional transplants but the use of biopolymer nanostructure and calcium phosphate composites of carbon apatite in PLA as scaffolds for tissue regeneration has not been sufficiently highlighted by the existing literature.

The objective of this work was the computational 4D printed design model development and characterisation of PLA/cHA scaffolds by the 3D printing technique, with the sole aim of using it for bone regeneration. This is followed by the microstructural analysis of the scaffolds by the computerised micro-tomography to determine roughness, morphological parameters of pore size distribution, porosity, as well as better visualisation of the distribution of particles. The PLA/cHA filaments were developed by the 3D printing technique to be used as raw material for the production of the scaffolds. Also, the microanalytical mechanical compression test was carried out to assess the strength of the scaffolds and to verify the effects of the incorporation of cHA on the properties of the biomaterial.

2. Materials and methods

2.1. Materials

The material and equipment were employed include the following; the PLA/cHA filaments in the mass ratios of 100/0, 95/5 and 80/20, a roller mixer, a Willey knife mill, A 3D printer and extruder assemble from part according to the procedure in Refs. [35,36]. A diffractometer for X-ray diffraction analysis, the Scanning Electron Microscope (SEM) coupled to a dispersive energy detector SEM/EDS for microstructures and charge dispersion analysis Form Mountain 8 premium (Digital surface software) for thermographic analysis where use according to Refs. [4,9,40].

2.2. Methods

The methodology employed in this work comprises of four steps namely the; cHA incorporation in PLA, EDX morphological characterization, determination of the apparent porosity and the in vitro degradation tests according to Refs. [3,25]. A compression test to evaluate the mechanical strength of the scaffolds and to verify if the incorporation of cHA improved the properties of the biomaterials was done following these literature procedures [35,40]. These are explained in details in the subsections below;

2.2.1. cHA incorporation in PLA

Initially, the carbon apatite (cHA) charge was incorporated into the polylactic acid (PLA) matrix with a PLA/cHA ratio of 95:5 m/m and 80:20 m/m using a roller mixer. After this process, the dough obtained was ground in a Willey knife mill, in order to obtain a suitable grain size for feeding into the extruder. 100/0 PLA was also processed under the same conditions for comparison purposes. The PLA and PLA/cHA (95:5 80:20 m/m) filaments were obtained coupled to a cooling coil and reel-type winder with the zone temperatures ranging between 170°C and 190 °C and thread rotational speed between 20 and 30 rpm. The following process steps were adopted for the production of 3D printing frameworks by the FDM technique. First, the computational model was produced using SolidWorks® software. The 3D geometry of the structure was constructed in the orientation of layers (0°–90°), as described in Figs. 1–2, with a cubic dimension of 4x6x6 mm for height, side and side, respectively. The printing parameters used include; 20 mm/s print speed, 0.3 mm layer thickness and 0°–90° deposition angle. These were entered into the Slic3r® software of the 3D printer and used to generate a file format g-code. The scaffolds were made from PLA/cHA filaments in the mass ratios of 100/0, 95/5 and 80/20 using a 3D printer at De Montfort University Mechanical Laboratory at a printer extrusion die temperature of 210 °C. The visual aspects and dimensional deviations of the scaffolds were thereafter evaluated. The filaments obtained in the extrusions, with an average diameter of 1.70 mm were used to feed the 3D printer. A CAD model of frame geometry with 0°–90° layer orientations and 4 mm × 6 mm x 6 mm dimension was previously made using
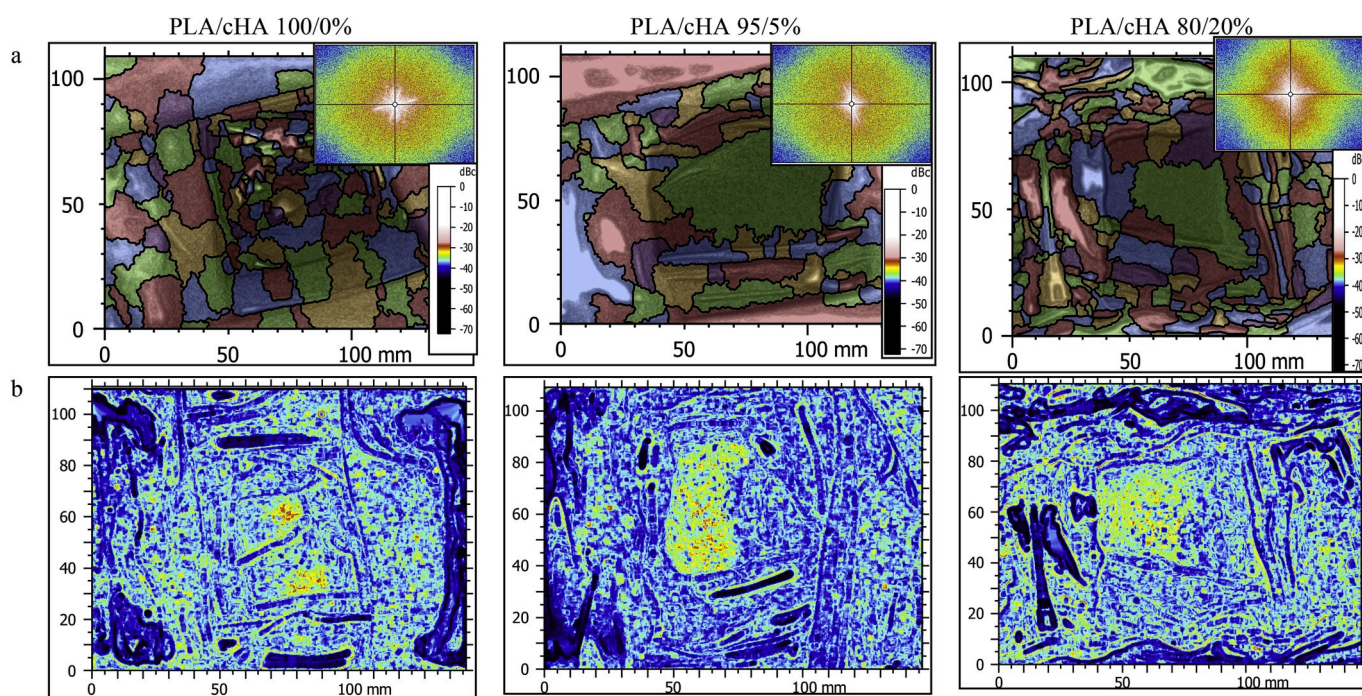

Fig. 2. (a)Particle microanalyses of Karhunen-Loeve (KL) transform and frequency spectrum of the image analysis (b) texture directional mapping properties in (Vm).

SolidWorks® software. The extrusion temperature of 210 °C, the print speed of 20 mm/s and the layer thickness of 0.3 mm were the printing parameters used.

2.2.2. EDX morphological characterization

The microstructural characterisations of PLA/cHA composites and pure carbon apatite were performed by X-ray diffraction analysis using a diffractometer, operated in a 2D scanning range of 5°–80° and continuous scan with 2°/min scan speed. For the XRD analysis, the specimens were printed with PLA/cHA filaments using the same printing parameters as the scaffolds. Thermogravimetric analyses were performed on Shimadzu TGA-50 equipment, in the heating range of 25 °C–80 °C, a heating rate of 10 °C/min, in the N2 atmosphere, in the matrix. Next is the composite loading of PLA in pellets and cHA powder, in the filaments and scaffolds of PLA/cHA in order to evaluate the thermal stability of the polymeric matrix and composites obtained in the light of the processing and load insertion in the obtained proportions. TG curves and the derivative of these curves (DTG) were obtained. The frameworks obtained by the FDM technique were characterised using the Scanning Electron Microscope (SEM) coupled to a dispersive energy detector SEM/EDS, in order to evaluate their microstructures and charge dispersion by the detection of calcium and phosphate groups. The external surface and cross-section fracture of the samples were evaluated. The isotropy for the value of the parameter of Fig. 1 is 34.22% having a first, second and third-degree direction of 88.47°, 95.77° and 7.744° respectively.

2.3. Biomaterials for bone regeneration

The materials can be conceptualised as a biomaterial because of the following reasons; (i) they are of natural origin, (ii) they are used in the medical field, or (iii) because they are susceptible to the action of microorganisms and biodegradable enzymes [32–34]. In this research biomaterials for application, bone regeneration was considered. In regard to their interaction with the organism, biomaterials can be classified as (i) bioinert materials that do not adhere to receptor tissue due to the formation of a fibrous capsule reaction (ii) biotolerant materials that adhere to receptor tissue, binding to them, but not performing a reactive function in this tissue, such as inducing cell growth and proliferation or (iii) bioactive [35,36]. A bioactive biomaterial has properties compatible with those of the tissue in which it will lodge, thus, stimulating an optimal response, and performing the function of repairing or replacing organs and tissues present in the human body. Bioactive materials can interact with natural tissues, causing reactions that favour the development of processes such as the implant fixation, bio-colonisation, host tissue regeneration or material biodegradation [37,38].

In tissue engineering, biomaterials are used as supports, with the scaffolds to guide and support cell growth, stimulating the regeneration of damaged tissue and playing the role of damaged tissue until it is recovered or regenerated. For the production of scaffolds, several criteria must be met, these include; (i) biocompatibility, (ii) surface suitable for tissue cell proliferation, (iii) mechanical properties similar to those of real bones and (iv)high porosity with pores interconnected by a network that allows cell growth, nutrient transport, and metabolic waste flow [39].

2.4. Apparent porosity

The apparent porosity of the scaffolds obtained was determined according to the ASTM F 2450-10 standard. Following the Archimede's principle, assuming that everybody soaked in a fluid undergoes a vertical upward force on the part of the liquid, an equal to the weight of the fluid is displaced by the body.

A hydrostatic balance was used to measure the mass of five samples of 100/0 PLA scaffolds and five examples of 5% dried and immersed PLA/cHA in ethanol. The masses of different samples were examined before and after immersion was used, together with ethanol density

($\rho_{ethanol}$), and the excellent the apparent density (D_{ap}) of the scaffolds as described in Equation (1) [40,41].

$$\text{Apparent density} \left(\text{Dap} \right) = \frac{M_{dry*} \; \rho_{ethanol}}{M_{wet} - M_{dry}} \tag{1}$$

The sample dimensions were measured with a calliper to determine the actual volume of the scaffolds (V_{real}), which was obtained by the cube volume formula. The pore volume (V_{pores}) is then measured according to the relationship described in Equation (2) for each of the samples [42].

$$\text{Apparent porosity} = \frac{V_{pores}}{V_{real}} \times 100 \tag{2}$$

According to Fig. 2, the watershed method was used to detect the number of particles in the composite which is set to 265 with a projected area of 60.45 μm^2 and a height of 9.49 nm.

2.5. In vitro degradation tests

In vitro degradation, analyses of the frameworks were conducted according to ISO 10993 (1994). The PLA/cHA scaffolds in the proportions of 100/0, 95/5 and 80/20 were immersed in a 45 mL of body fluid simulation. The tests were performed with the solution at different pHs. The pH of the solutions was adjusted to 7.4 pH of physiological solution and 4.0 pH of an inflammatory response by the addition of lactic acid. The scaffolds were kept immersed in the solution for different hours in an incubator as described by Refs. [42–44]. The assay was performed in triplicate for each PLA/cHA composition, different incubation time and pH. After each observation time, the scaffolds were removed. The calcium (Ca) and phosphorus (P) content present in the solutions was quantified by the Microstructural Emission Spectrometry (MES) technique, performed with the Digital Surface Software (Mountain 8 Premium).

3. Results and discussion

The micrographs obtained from the Scanning Electron Microscopy (SEM) analysis, as well as the mapping and graph of charge quantification present in the EDS framework, are described in Figs. 1 and 2. The Figures show the filament integrity of the obtained scaffolds and its geometry to the projected model, although the insertion of the charge to the polymeric matrix composite seems to have hindered the free flow of deposition of filaments since some irregularities were noticed in the surface rugosity roughness (Fig. 3A). The micrographs of the cross-sections of the scaffolds shown in Fig. 3 showed a flatness in the loaded material when compared to the 100/0 PLA scaffolding. This effect may be linked to the high density of carbon apatite is 3.0 g/cm^3 when compared to the mass of the PLA matrix composite of 1.25 g/cm^3, generating a flattening by weight. Comparing the micrographs it is still possible to say that a decrease in pore size occurred which was confirmed by the results of the apparent porosity analysis. The graphs of EDS presented in Fig. 3a elucidate the presence of carbon (C) and oxygen (O) related to PLA and also the presence of calcium (Ca) and phosphorus (P) related to cHA. The EDS mappings and spectra for the PLA/cHA scaffolds in the proportions 95/5 and 80/10, respectively are represented in Fig. 3. All the furrows of cells density are shown in Fig. 3B with different texture direction. The mean depth of furrows parameters and mean density of furrows for the composite sample of cHA 0%, 5% and 20% are 22.06 nm, 25.2 nm, and 27.21 nm with 3.364 cm/cm^2, 3.408 cm/cm^2 and 4.102 cm/cm^2 respectively. The isotropy parameters value and the average directional texture were measured to be 31.32%, 45.05% and 57.88% with 20.47°, 64.1° and 91.73° respectively according to Fig. 3. The spacing parameters of roughness profile was done according to ISO 4287 having a Gaussian filter of 0.8 μm evaluation length and a peak parameters surface roughness profile rugosity according to Fig. 3b. The microanalysis material ratio parameters of a
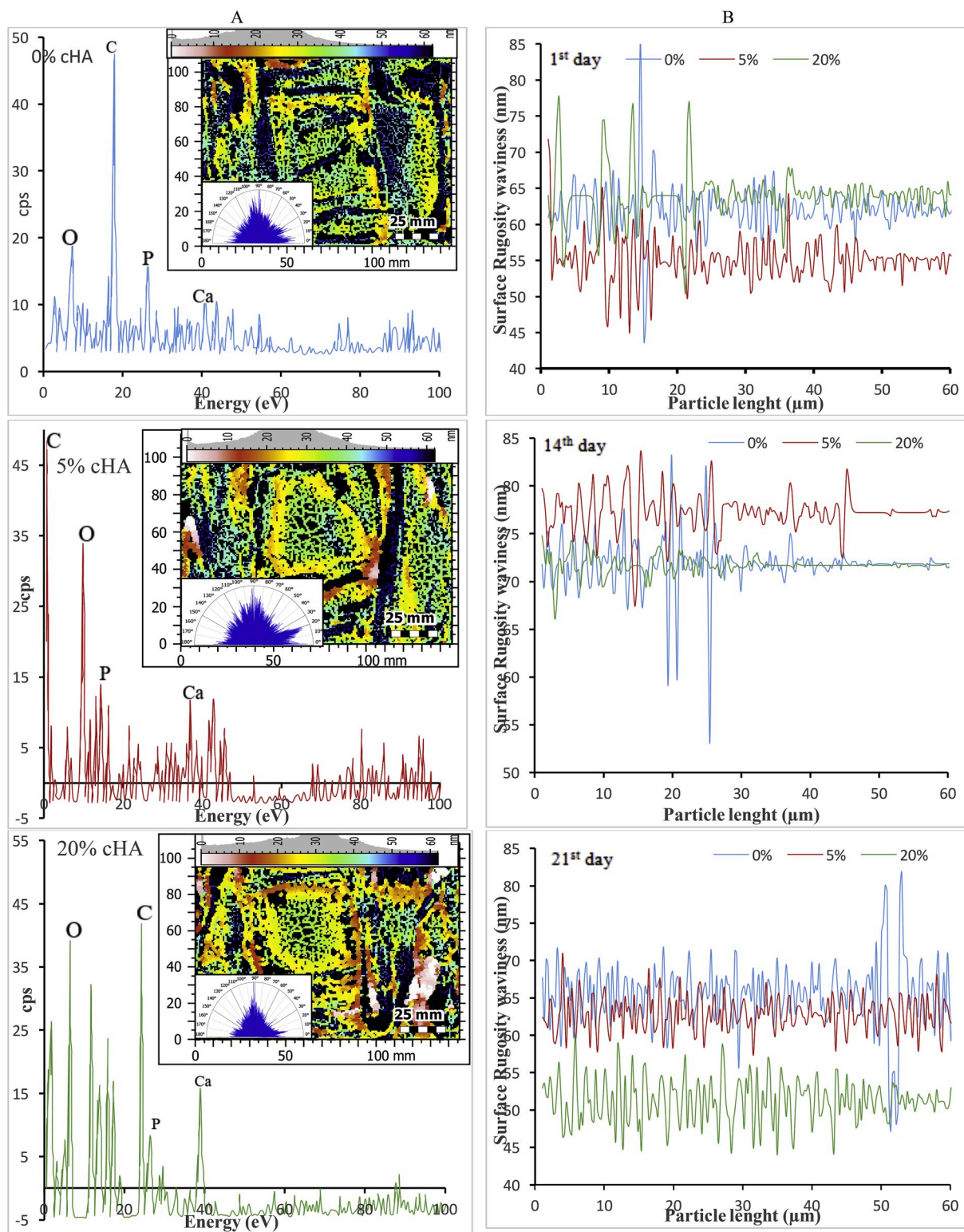
Fig. 3. The graphs of the different scaffold of the composite of cHA in 0%, 5%, and 20% (a) EDS of surface and cross-section of cells density of furrows with texture movement direction (b) Rugosity of surface roughness of day 1, 14 and 21.

primary profile record 100%.

The results presented by the graphs show the presence of charge not only on the surface of the scaffolds (Fig. 4A) but also in the inside, with proportional Ca and P concentrations, making clear the efficiency of the whole structure. The process of obtaining these scaffolds from the mixture for the incorporation of the load to the printing process as well as the carbon apatite dispersion in the polymer matrix and filament

homogeneity of the PLA/cHA scaffolds are illustrated in Fig. 4. According to the mapping performed by EDS with detection of atoms of the elements Calcium (Ca) and Phosphorus (P), it was possible to demonstrate that the carbon apatite charge was efficiently incorporated into the PLA polymer matrix. It is also possible to notice a homogeneous dispersion of this charge without the presence of agglomerates of the same. These results reinforced the effective load dispersion in the
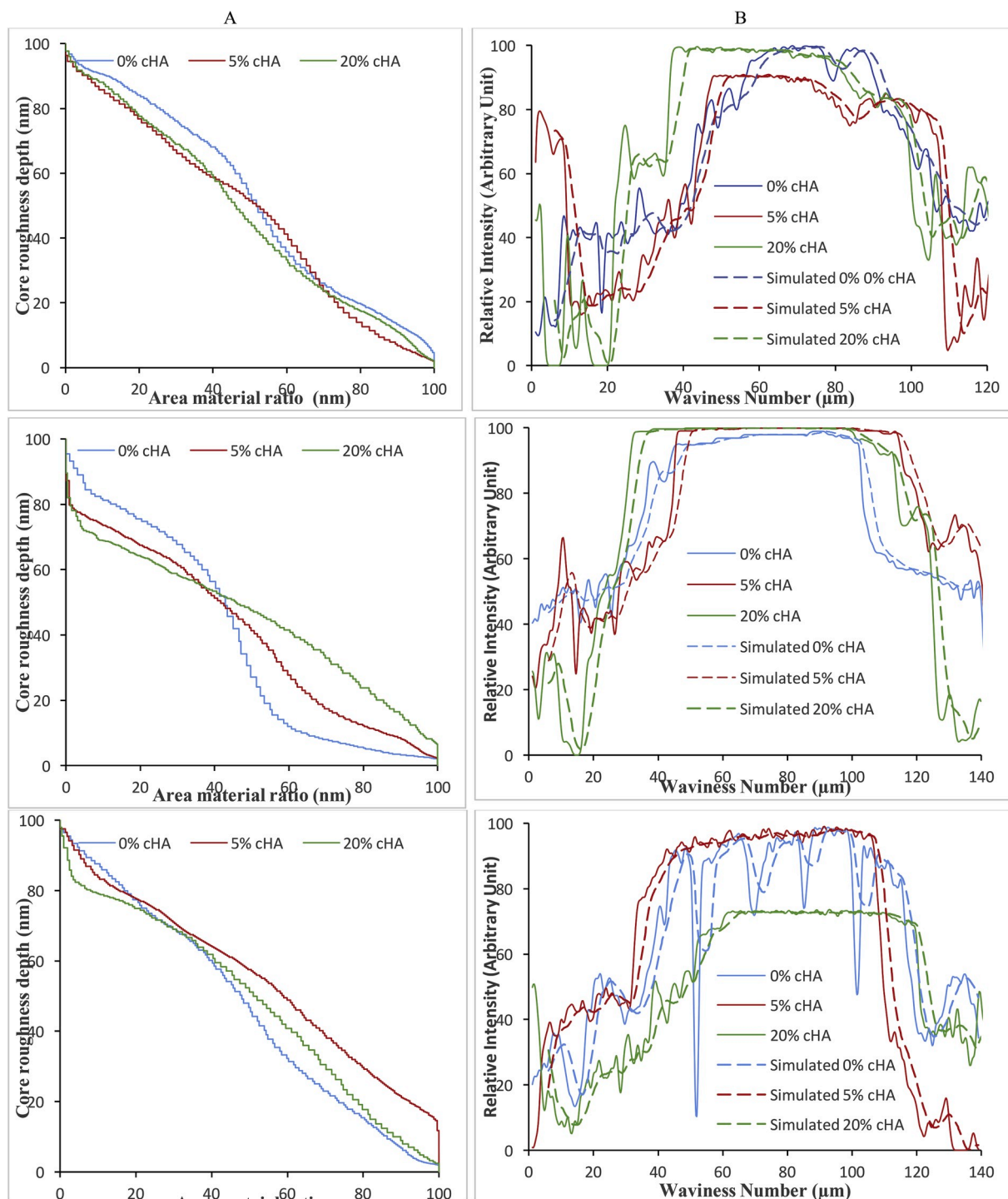
Fig. 4. The graphical representation of in 1st 14th and 21st day (a) the scale fractal microanalysis of peak count distribution in core roughness depth of the material ratio (b) Waviness analysis of the level scale erosion filter of the samples.

developed composite. Therefore, the apparent porosity of the harnessed proof scaffold experimental data calculated to obtain apparent porosity is shown in Table 1.

The apparent porosity of the 5% and 20% of cHA scaffolds were determined, and a porosity percentage of approximately 62% and 41% were found respectively. To the 0% of cHA frameworks, the apparent porosity value remained at an average of 71%. The results reveal a possible effect of the load on the porosity of the scaffolds, as previously mentioned in the micrograph results, where the hypothesis of the load weight in the matrix caused the filament flattening, and consequently,

Table 1

Apparent porosity of harness proof scaffold experimental data calculated to obtain apparent porosity.

Scaffold	Dry mass (g)	Wet mass (g)	Real volume (cm³)	Volume of porosity (cm³)	Apparent density (g/cm³)	Porosity (%)
cHA 0%	0.065	0.10	0.150	0.1147	1.439	76.47
cHA 5%	0.072	0.12	0.153	0.1072	2.082	70.06
cHA 20%	0.085	0.17	0.179	0.092	2.772	51.40

the pore shrinkage was raised. Equation C directly correlates porosity percentage with pore volume, and it is correct to state that the reduction of porosity in the scaffolds was due to the lower pore volume of the PLA/cHA 95: 5 scaffolds. The porosity values of the scaffolds, as well as the effect of apatite load insertion on the porosity reduction, are in agreement with the values described in Ref. [42].

The effect of carbon apatite loading on the PLA/cHA scaffolds geometry was observed earlier in Fig. 2, From the SEM of the scaffolds, it was possible to notice a flattening of the deposited PLA filaments during printing. This flattening, possibly due to the weight of the charge in the matrix, led to a reduction in pore size, thereby, reducing its volume. Equation (1) directly relates porosity percentage to pore volume, suggesting that the decrease in scaffold porosity is related to the high density of carbon apatite. Its thickness can also be observed by increasing the dry mass of PLA/cHA scaffolds proportional to the increase of cHA content. It was also observed that the increase of 5%–10% in the PLA/cHA scaffolds did not change its porosity and that this load insertion increased the scaffold size variation, since the standard deviation for the scaffolds. Carbapatite specimens were larger when compared to unloaded scaffolds. The filtered profiles cut-off were too
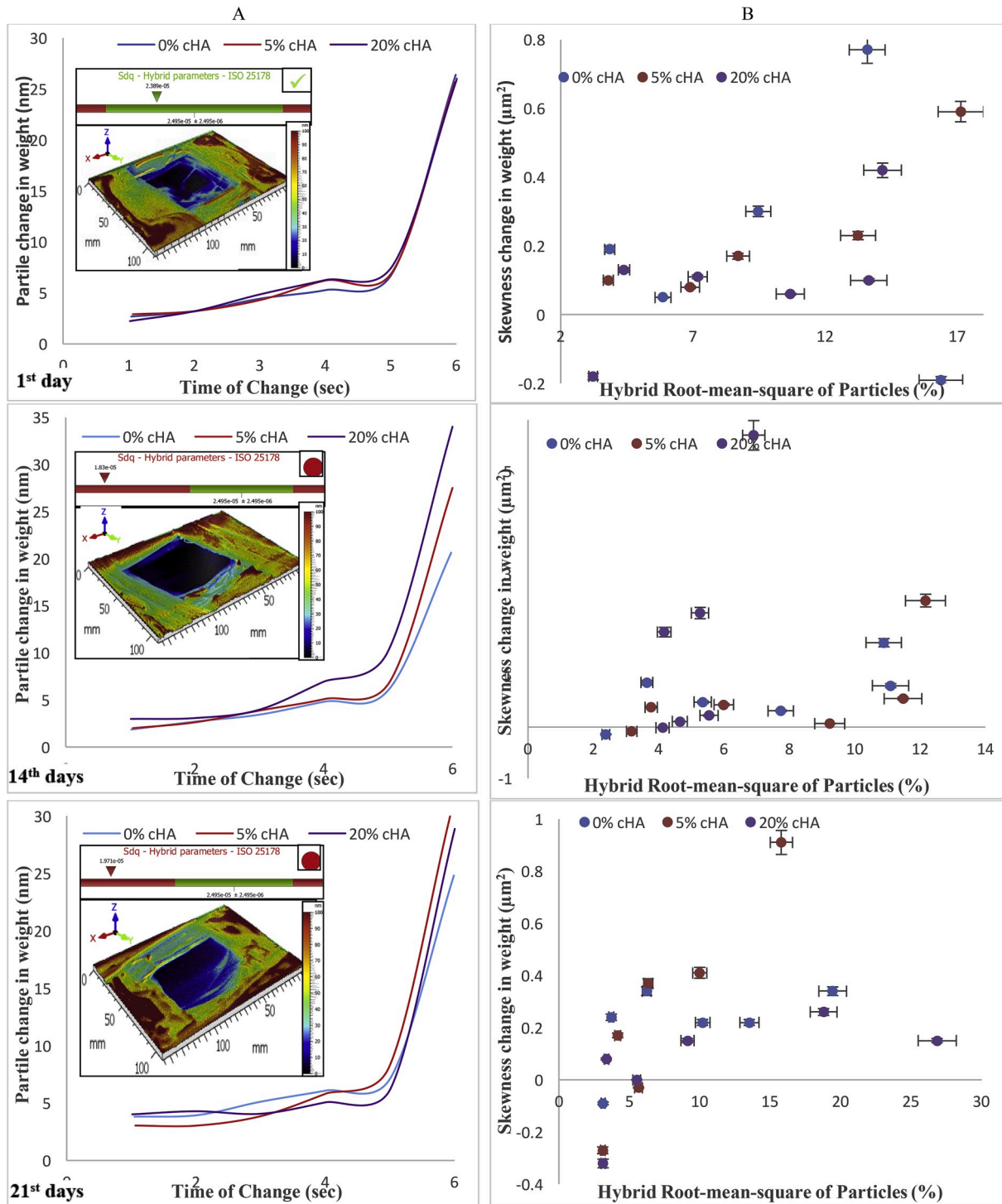

Fig. 5. A graph for the 1st, 14th and 21st days (A) Change in weight of nanoparticle with time (B) Skewness change in weight of the hybrid root-mean squareness of the nanoparticles.

small for microanalysis, hence, mthe sampling lengths are used. It gives a resultant profile waviness of filter settings in Gaussian filter of cut-off 2.5 μm, and 1/2 cut-off at each end of the sample was removed according to Fig. 4A and B.

According to Fig. 5, the first day core roughness depth (Sk) parameters of the area of the material ratio of a Gaussian filter (0.8 μm stratified surfaces) of the filter settings gives a core roughness depth (Sk) of 78.80 nm. The reduced summit height, reduced valley depth and the percentage upper and lower bearing area difference of the samples are 16.33 nm, 9.62 nm and 75.07% respectively. The arithmetic means that the height is 1.142P, and volume of 1012 $nm^3/\mu m^2$ having a peak volume material, core material, core void, and pit core volumes of $4.87 \times 10^{-7} \mu m^3/\mu m^2$, 3.097e-057 $\mu m^3/\mu m^2$, $4.24 \times 10^{-5} \mu m^3/\mu m^2$ and $2.11 \times 10^{-6} \mu m^3/\mu m^2$ respectively. The porosity values of the scaffolds, as well as the effect of apatite load insertion on the porosity reduction, are in agreement with the range of values found and the load effect described by Refs. [39–42]. Further analyzes were also performed on the PLA/cHA 95/5 and 80/10 scaffolds after 672 h release at pH 7.4 and 4.0, to assess whether there was a change in the intensity of Ca and P peaks in the spectra. Fig. 5A and B and Fig 3A show the EDX spectra of the surfaces and cross-sections of the scaffolds. The EDX spectra showed no change in the intensity of the Ca and P element peaks in the PLA/cHA scaffolds before and after 21day release at both pHs (pH 7.4 and 4.0). Thus, it can be inferred that although there was a release of these elements, EDX was not an ideal analysis to elucidate this release in the studied Ca and P concentrations. The root-mean-square gradient (Sdq) has a value of 8.99×10^6 with a developed interfacial area ratio (Sdr) of 4.89×10^{-9}% which is significantly small and a skewness value of 0.102. In the control chart of the particle analysis using ISO 25178 according to Fig. 5B, the variance, parameters have a value of 65.15 nm^2 with a yield percentage of 66.67% and process capability (Cp) which is 0.3413. The process capability index (Cp) on the control chart which is the statistical process control measurement of process capability is 0.2470. The performance charts (Cpk), has the same value as Cp and the process capability index unit length (Cpku) is 0.4357 with an Engineering Tolerance (ET) of 16.53 nm^2, and Neutral Tolerance (NT) of 48.43 nm^2. The ratio of ET/NT gives the critical value of Cp to be 0.3413 according to Fig. 5B.

A comparison can be made between the 100/0 framework and the 95/5 and 80/10 frameworks regarding the effect of load insertion on the framework geometry. In the micrographs of the cross-sections of Fig. 5, it is possible to observe a flattening of the deposited filaments, resulting in a reduction in pore size, which for the PLA/cHA 100/0 framework is approximately 330 μm (±2 μm), while for the PLA/cHA 95/5 and 80/10 frameworks it was around 290 ± 1.67 μm. Approximately 13% reduction in pore size in two dimensions (represented by the distance between the filaments deposited) from cHA-free scaffolds of 100/0 to cHA, 95/5 and 80/10 scaffolds were noted. The micrograph shown in Fig. 5 of a PLA/cHA 80/10 framework with higher carbon apatite content shows particles smaller than their average diameter in their received product form average diameter of approximately 90 μm. The parameters table for KL transformed of the 4D failure particle microanalysis testing according to ISO 25178 is represented in Table 2. This result indicates that in addition to no charge agglomeration, the expected effect when there is little or no charge interaction with the matrix in the composite, is that the carbon apatite particles suffered breaks during the scaffolding process. Smaller carbon apatite particles can potentiate their effect on the scaffolds as the contact surface, and the broad area of the particles in the polymer matrix will be more significant.

The micrographs also show a compromise in filament accuracy and integrity, especially for cHA-containing scaffolds. CHA-containing filaments showed not-so-continuous flow (more turbulent flow) at the time of printing compared to pure PLA filament more laminar flow, which probably interfered with the accuracy of the printed scaffolds. The size of the scaffolds has also become a challenge in printing, as tiny pieces make printing difficult. The defects presented in the present work were found in the literature in samples of polycarbonate and ABS blends by Ref. [37]. According to the authors, these effects were due to printing parameters, such as the thickness of the deposited layers of the filaments, the greater deposition angle of the layers and the small interaction between the framework constituent materials, as shown in Fig. 5. It is noteworthy the importance of the results presented in the EDX analysis since the presence of Ca and P on the surface of the scaffolds will be essential for the biological performance of the biomaterial, while the presence of the load internally in the scaffolds may lead to improved mechanical strength.

4. Conclusion

The results presented in this work showed that it is possible to produce 95/5 PLA/cHA composite scaffolds by melt mixing, extrusion and 3D printing techniques, with morphology and charge dispersion suitable for the intended application. The micrographs of the cross-sections of the scaffolds showed a flatness in the loaded material when compared to the 100/0 PLA. Furthermore, the apparent porosity of the 5% and 20% of cHA scaffolds gave a porosity percentage of approximately 62% and 41% respectively. The reduced summit height, reduced valley depth and

Table 2
Parameters table KL transformed of the 4D failure particle microanalysis testing according to ISO 25178.

Materials Properties	Tolerances and Unit	Parameters testing 4D particles					
		cHA 0%		cHA 5%		cHA 20%	
Root-mean-square height (sq)	22.96 ± 2.296 nm	27.91	Fail	33.75	Fail	31.33	Fail
Skewness (Ssk)	−0.5511 ± 0.05511	0.04941	Fail	−0.179	Fail	−0.1543	Fail
Kurtosis (Sku)	2.780 ± 0.2780	1.997	Fail	1.684	Fail	1.782	Fail
Maximum peak height (Sp)	39.17 ± 3.917 nm	53.35	Fail	45.01	Fail	51.87	Fail
Maximum pit height (Sv)	60.83 ± 6.083 nm	46.65	Fail	54.99	Fail	48.13	Pass
Maximum height (Sz)	100.0 ± 10.00 nm	100.0	Pass	100.0	Pass	100.0	Pass
Arithmetic mean height (Sa)	18.58 ± 1.858 nm	23.36	Fail	29.49	Fail	27.01	Fail
Functional and Spatial parameters							
Areal material ratio (Smr)	100.0 ± 10.00%	100.0	Pass	100.0	Pass	100.0	Pass
Inverse areal material ratio (Smr)	27.86 ± 2.786 nm	39.68	Fail	45.00	Fail	41.77	Fail
Extreme peak height (Sxp)	58.26 ± 5.826 nm	47.93	Fail	57.63	Fail	50.54	Pass
Autocorrelation length (Sal)	9.578 ± 0.9578 μm	30.66	Fail	33.05	Fail	23.11	Fail
Texture direction (Std)	63.24° ± 6.324°	8.248	Fail	4.997	Fail	22.11	Fail
Hybrid and Functional parameters							
Root-mean-square gradient (Sdq)	$2.50 \times 10^{-5} \pm 2.50 \times 10^{-5}$	2.58×10^{-5}	Pass	1.97×10^{-5}	Fail	3.47×10^{-5}	Fail
Developed interfacial area ratio (Sdr)	$3.11 \times 10^{-8} \pm 3.11 \times 10^{-9}$%	3.33×10^{-8}	Fail	1.94×10^{-8}	Fail	5.81×10^{-8}	Fail
Material volume (Vm)	$6.43 \times 10^{-7} \pm 6.43 \times 10^{-8} \mu m^3/\mu m^2$	6.71×10^{-7}	Fail	1.0×10^{-9}	Fail	5.47×10^{-7}	Fail
Void volume (Vv)	$2.85 \times 10^{-5} \pm 2.85 \times 10^{-6} \mu m^3/\mu m^2$	4.04×10^{-5}	Fail	4.5×10^{-5}	Fail	4.23×10^{-5}	Fail
Peak material volume (Vmp)	$6.42 \times 10^{-7} \pm 6.42 \times 10^{-8} \mu m^3/\mu m^2$	6.71×10^{-7}	Fail	1.0×10^{-9}	Fail	5.46×10^{-7}	Fail
Core material volume (Vmc)	$2.40 \times 10^{-5} \pm 2.40 \times 10^{-5} \mu m^3/\mu m^2$	3.09×10^{-5}	Fail	4.15×10^{-5}	Fail	4.07×10^{-5}	Fail

the percentage upper and lower bearing area difference of the samples are 16.33 nm, 9.62 nm and 75.07% respectively. The EDX spectra showed no change in the intensity of the Ca and P element peaks in the PLA/cHA scaffolds before and after 21day thus, it can be inferred that although there was a release of these elements, EDX was not an ideal analysis to elucidate this release in the studied Ca and P concentrations. Approximately 13% reduction in pore size in two dimensions as represented by the distance between the filaments deposited from cHA-free scaffolds of 100/0 to cHA, 95/5 and 80/10 scaffolds were observed. According to the release of Ca and P in the EDX, longer incubation times was achieved when using dynamic condition reactor to simulate the stresses suffered by the biomaterial exerted by the flow of body fluids. Also a microstructural analysis of the scaffolds by 3D printing and computerised microtomography to determine roughness, morphological parameters of pore size distribution, porosity as well as better visualisation of the distribution of loads is possible. These results and findings are applicable in many biomaterials industries in the development of biomaterials which have been engineered with biological systems to meet medical purposes.

Declaration of competing interest

The authors declare that they have no known competing financial interests or personal relationships that could have appeared to influence the work reported in this paper.

Acknowledgment

References

[1] M. Karimi, R. Kalantarzadeh, G. Saba, T.M. Hafshejani, M. Shamsi, V. Jahangir, A. Jodaei, A. Sadeghinik, Apacite nanocomposites: a novel bioactive, biocompatible and osteogenic product originated from atmospheric carbon dioxide processed spontaneously in Calcoline, Chem. Eng. J. 353 (2018) 679–688.

[2] M. Bohner, Design of ceramic-based cements and putties for bone graft substitution, Eur. Cells Mater. 20 (2010) 1–12.

[3] J.O. Akindoyo, M.D.H. Beg, S.B. Ghazali, M.R. Islam, A.A. Mamun, Preparation and characterization of poly (lactic acid)-based composites reinforced with poly dimethyl siloxane/ultrasound-treated oil palm empty fruit bunch, Polym. Plast. Technol. Eng. 54 (13) (2015) 1321–1333.

[4] B.I. Oladapo, A.O.M. Adeoye, M. Ismail, Analytical optimisation of a nanoparticle of microstructural fused deposition of resins for additive manufacturing, Compos. B Eng. 150 (1) (2018) 248–254.

[5] C.O. Ijagbemi, B.I. Oladapo, H.M. Campbell, C.O. Ijagbemi, Design and simulation of fatigue analysis for a vehicle suspension system (VSS) and its effect on global warming, Procedia Eng. 159 (2016) 124–132.

[6] A.O.M. Adeoye, J.F. Kayode, B.I. Oladapo, S.O. Afolabi, Experimental analysis and optimization of synthesized magnetic nanoparticles coated with PMAMPC-MNPs for bioengineering application, St. Petersburg Polytech. Univ. J.: Phys. Math. 3 (4) (2017) 333–338.

[7] R.A. Ilyas, S.M. Sapuan, M.R. Ishak, Isolation and characterization of nanocrystalline cellulose from sugar palm fibres (Arenga Pinnata), Carbohydr. Polym. 181 (2018) 1038–1051.

[8] R.A. Ilyas, S.M. Sapuan, R. Ibrahim, H. Abral, M.R. Ishak, E.S. Zainudin, A.M. N. Azammi, Sugar palm (Arenga pinnata (Wurmb.) Merr) cellulosic fibre hierarchy: a comprehensive approach from macro to nanoscale, J. Mater. Res. Technol. 8 (3) (2019) 2753–2766.

[9] B.I. Oladapo, S.A. Zahedi, A.O.M. Adeoye, 3D printing of bone scaffolds with hybrid biomaterials, Compos. B Eng. 158 (2019) 428–436.

[10] B.I. Oladapo, S.A. Zahedi, F. Vahidnia, O.M. Ikumapayi, M.U. Farooq, Three-dimensional finite element analysis of a porcelain crowned tooth, Beni-Suef Univ. J. Basic Appl. Sci. 7 (4) (2019) 461–464.

[11] B.I. Oladapo, S.A. Zahedi, S.C. Chaluvadi, S.S. Bollapalli, M. Ismail, Model design of a superconducting quantum interference device of magnetic field sensors for magnetocardiography, Biomed. Signal Process. Control 46 (2019) 116–120.

[12] Bankole I. Oladapo, S. AbolfazlZahedi, FrancisT. Omigbodun, Edwin A. Oshin, Victor A. Adebiyi, Olaoluwa B. Malachi, Microstructural evaluation of aluminium alloy A365 T6 in machining operation, J. Mater. Res. Technol. 8 (3) (2019) 3213–3222.

[13] X. Wang, W. Deng, L. Shen, M. Yan, J. Yu, A 3D electrochemical immune device based on an Au paper electrode and using Au nanoflowers for amplification, New J. Chem. 40 (2016) 2835–2842.

[14] R.L. Truby, J.A. Lewis, Printing soft matter in three dimensions, Nature 540 (2016) 371–378.

[15] R.A. Ilyas, S.M. Sapuan, M.R. Ishak, E.S. Zainudin, Development and Characterization of Sugar Palm Nanocrystalline Cellulose Reinforced Sugar Palm Starch Bionanocomposites Carbohydr Polym, vol. 202, 2018, pp. 186–202.

[16] B.I. Oladapo, A.V. Adebiyi, I.E. Elemure, Microstructural 4D printing investigation of ultra-sonication biocomposite polymer, J. King Saud Univ. Eng. Sci. (2019), https://doi.org/10.1016/j.jksues.2019.12.002. In press.

[17] A.J. Benítez, F. Lossada, B. Zhu, T. Rudolph, A. Walther, Understanding toughness in bioinspired cellulose nanofibril/polymer nanocomposites, Biomacromolecules 17 (2016) 2417–2426.

[18] K. Fu, Y. Yao, J. Dai, L. Hu, Progress in 3D printing of carbon materials for energy-related applications, Adv. Mater. 29 (2017), 1603486.

[19] J. Boetker, J.J. Water, J. Aho, L. Arnfast, A. Bohr, J. Rantanen, Modifying release characteristics from 3D printed drug-eluting products, Eur. J. Pharm. Sci. 90 (2016) 47–52.

[20] J. Goole, K. Amighi, 3D printing in pharmaceutics: a new tool for designing customized drug delivery systems, Int. J. Pharm. 499 (2016) 376–394.

[21] M.J. Halimatul, S.M. Sapuan, M. Jawaid, M.R. Ishak, R.A. Ilyas, Effect of sago starch and plasticizer content on the properties of thermoplastic films: mechanical testing and cyclic soaking-drying, Polimery 6 (2019) 422.

[22] Hairul Abral; Azmi Basri; Faris Muhammad; Yuzalmi Fernando; Fadli Hafizulhaq; Melbi Mahardika; Eni Sugiarti; S. M. Sapuan; R. A. Ilyas; Ilfa Stephane , A simple method for improving the properties of the sago starch films prepared by using ultrasonication treatment, Food Hydrocolloids, ISSN: 0268-005X, Vol: 93, Page: 276-283.

[23] M.S.N. Atikah, R.A. Ilyas, S.M. Sapuan, M.R. Ishak, E.S. Zainudin, R. Ibrahim, A. Atiqah, M.N.M. Ansari, R. Jumaidin, Degradation and physical properties of sugar palm starch/sugar palm nanofibrillated cellulose bionanocomposite, Polimery 10 (2019) 680.

[24] M.J. Halimatul, S.M. Sapuan, M. Jawaid, M.R. Ishak, R.A. Ilyas, Water absorption and water solubility properties of sago starch biopolymer composite films filled with sugar palm particles, Polimery 9 (2019) 595.

[25] A. Ficai, E. Andronescu, G. Voicu, M.G. Albu, A. Ilie, Biomimetically synthesis of collagen/hydroxyapatite composite materials, Mater. Plast. 47 (2010) 205–208.

[26] J.M. Williamsa, A. ADdewunmi, C.L. Flanagan, Bone tissue engineering using poly scaffolds fabricated via selective laser sintering, Biomaterials 26 (2005) 4817–4827.

[27] A. Tahmasbi Rad, M. Solati-Hashjin, N.A. Abu Oman, S. Faghihi, Improved bio-physical performance of hydroxyapatite coatings obtained by electrophoretic deposition at dynamic voltage, Ceram. Int. 40 (2015) 12681–12691.

[28] R.A. Ilyas, S.M. Sapuan, M.R. Ishak, E.S. Zainudin, Sugar palm nanofibrillated cellulose (Arenga pinnata (Wurmb.)Merr): effect of cycles on their yield, physic-chemical, morphological and thermal behaviour, Int. J. Biol. Macromol. 123 (2019) 379–388.

[29] M.L. Sanyang, R.A. Ilyas, S.M. Sapuan, R. Jumaidin, Sugar palm starch-based composites for packaging applications, in: M. Jawaid, S. Swain (Eds.), Bionanocomposites for Packaging Applications, Springer, Cham, 2018.

[30] R.A. Ilyas, S.M. Sapuan, M.R. Ishak, E.S. Zainudin, Sugar palm nanocrystalline cellulose reinforced sugar palm starch composite: degradation and water-barrier properties, Mater. Sci. Eng. 368 (2018) 6–12.

[31] L. Sanyang, R.A Ilyas, S,M, Sapaun and R. Jumaidin. Sugar palm starch-based composites for packing applications.M. Swain (Eds) Bionanocomposites for Packing Applications; Springers, Chem. pp. 125-147.

[32] P.M. Arockianathan, S. Sekar, S. Sankar, B. Kunkran, T.P. Sastry, Evaluation of biocomposite films containing alginate and sago stain impregnated with silver nano particles, Carbohydr. Polym. 90 (1) (2012) 717–724.

[33] M.S.N. Atikah, R.A. Ilyas, S.M. Sapaun, M.R. Ishak, E.S. Zainudin, R. Ibrahim, A. Atiqah, M.N.M. Ansari, R. Jumaidin, Degradation and physical properties of sugar palm starch/sugar palm nano fibrillated cellulose binano composite, Polimery 64 (10) (2019) 27–36.

[34] E. Glowinska, J. Datta, Structure, morphological and mechanical behaviour of novel bio based poly urethane composite with micro crystalline cellulose, Cellulose 24 (4) (2015) 2471–2481.

[35] K. Szustakiewicz, B. Stępak, A.J. Antończak, M. Maj, M. Gazińska, B. Kryszak, J. Pigłowski, Femtosecond laser-induced modification of PLLA/hydroxypatite composite, Polym. Degrad. Stab. 149 (2018) 152–161.

[36] A. Oryan, M.B. Eslaminejad, A. Kamali, S. Hosseini, A. Moshiri, H. Baharvand, Cell Tissue Res. 374 (2018) 63–81.

[37] M. Lebourg, J.S. Antón, J.G. Ribelles, J. Mater. Sci. Mater. Med. 21 (2010) 33–44.

[38] B. Rentsch, R. Bernhardt, D. Scharnweber, W. Schneiders, S. Rammelt, C. Rentsch. Biomater. 2 (2012) 158–165.

[39] M. Shahrezaee, M. Salehi, S. Keshtkari, A. Oryan, A. Kamali, B. Shekarchi, Nanomedicine 14 (2018) 2061–2073.

[40] Shadi Hassanajili, Ali Karami-Pour, Oryan Ahmad, Tahereh Talaei-Khozani, Preparation and characterization of PLA/PCL/HA composite scaffolds using indirect 3D printing for bone tissue engineering, Mater. Sci. Eng. C 104 (November 2019). Article 109960.

[41] Francis T. Omigbodun, Bankole I. Oladapo, Oluwole K. Bowoto, Funso P. Adeyekun, Experimental model design and simulation of air conditioning system for energy management, Int. Res. J. Eng. Technol. 6 (6) (2019) 811–816.

[42] Francis T. Omigbodun, Bankole I. Oladapo, Oluwole K. Bowoto, Funso P. Adeyekun Modelling detection of magnetic hysteresis properties with a microcontroller, Int. J. Eng. Trends Technol. 67 (6):5-12.

[43] V.A. Balogun, B.I. Oladapo, Electrical energy demand modeling of 3D printing technology for sustainable manufacture, Int. J. Eng. 29 (7) (2019) 1–8.

[44] B.I. Oladapo, A.S. Zahedi, S. Chong, F.T. Omigbodun, I.O. Malachi, 3D printing of surface characterisation and finite element analysis improvement of PEEK-HAP-GO in bone implant, Int. J. Adv. Manuf. Technol. 13 (1) (2019), https://doi.org/10.1007/s00170-019-04618-w.